Direct Observation of Internal Structures in Poly(*N*-isopropylacrylamide) Chemical Gels

Yoshitsugu Hirokawa,[†,‡] Hiroshi Jinnai,[†,§] Yukihiro Nishikawa,[†,∥] Takuya Okamoto,[†,‡] and Takeji Hashimoto*[,†,⊥]

Hashimoto Polymer Phasing Project, ERATO JST, and Department of Polymer Chemistry, Graduate School of Engineering, Kyoto University, Kyoto 606-8501, Japan

Received March 23, 1999; Revised Manuscript Received August 16, 1999

ABSTRACT: Internal structures of translucent poly(*N*-isopropylacrylamide) gel were for the first time observed by laser scanning confocal microscopy (LSCM). The observed image reflected the mesoscopic internal structures in the gel due to the "fixed concentration fluctuations" of network polymers as described in the text. Three-dimensional internal structures in the gel constructed from a series of the cross section images taken by the LSCM revealed that the gel had a bicontinuous domain structure consisting of regions dense and sparse in polymer networks.

I. Introduction

Polymer gels are three dimensionally cross-linked polymer networks containing fluid. They are versatile materials whose peculiar characteristics are utilized for various applications. The characteristics of gels, such as optical, mechanical, thermal properties, etc. are related to the internal structures of the gels. Extensive studies have been made on the characterization of the gels,[1,2] and the gels have long been considered to be composed of by and large uniform networks. In recent years, however, the significance of inhomogeneities of the polymer gels has been recognized, and there have been an increasing number of reports concerning the spatial inhomogeneities of polymer gels.[3−16]

Weiss and Silberberg reported that the high permeability of polyacrylamide gels was attributed to the inhomogeneities of the gel network.[3] Tanaka et al. pointed out that the inhomogeneities of gels were mainly coming from the two origins on the basis of the light-scattering measurements.[13] One is due to the formation of the inhomogeneities fixed in the gel during the gelation process: As the gelation reaction proceeds under certain gelation conditions, the resultant linear and branched polymers exhibit critical concentration fluctuations or undergo domain formation due to the phase separation. The fluctuations or the domains are then fixed by cross-linking, yielding static (or fixed) inhomogeneities. They may form a sort of internal structure permanently trapped in the gel. Another origin is due to the dynamic inhomogeneities, i.e., the dynamic thermal concentration fluctuations of the polymer network with their amplitudes and relaxation times depending on the position in the phase diagram of the gel.

As for the real space analyses of the static inhomogeneities, that is, internal structures, there are few reports. Recently, Suzuki et al. applied an atomic force microscopy to observe the surface of polymer gel and found spongelike domains with a submicrometer scale.[16] This is an important piece of information about the gel surface but the internal structures of the gel still remain unsolved.

In the present study, we focused on the internal structures in gels caused by the static inhomogeneities. To unveil the internal structures of translucent poly(*N*-isopropylacrylamide) gels, direct observation of the structures was carried out for the first time by means of laser scanning confocal microscopy (LSCM). LSCM does not require any elaborated pretreatments of a sample, which are necessary for observation under transmission electron microscopy. Therefore, we can achieve in situ observation of the internal structures of the gel without imposing any perturbations on the sample. Furthermore, LSCM has an advantage that the image only coming from the focal plane is detected, allowing us to overcome the difficulties associated with smearing of images due to an overlap of structures along the depth direction of the sample. A series of optically sliced images observed at different depths in the sample along with the aid of computational stacking[17,18] makes it possible to construct the three-dimensional digital images of the internal structures.

II. Experiments

1. Materials. *N*-Isopropylacrylamide (NIPAAm) (Tokyo Kasei) was purified by the recrystallization, which was performed by pouring the NIPAAm toluene solution into a large amount of *n*-hexane. *N*,*N*′-Methylenebis(acrylamide) (BIS) (Wako, electrophoresis grade), *N*,*N*,*N*′,*N*′-tetramethylethylenediamine (TEMEDA) (Wako, electrophoresis grade), ammonium peroxodisulfate (AP) (Wako, electrophoresis grade), and 8-anilino-1-naphthalene sulfonic acid ammonium salt (ANSA) (Wako) were used without any further purification. The ANSA had a maximum adsorption wavelength of 364 nm and a maximum emission wavelength of 482 nm in methanol.

2. Gel Preparation. A monomer solution was prepared by dissolving NIPAAm (0.7524 g) (a main constituent), BIS (7.71 mg) (a cross-linker), and TEMEDA (12.0 μL) (an accelerator)

* To whom correspondence should be addressed at Kyoto University.
† Hashimoto Polymer Phasing Project, ERATO JST.
‡ Present address; Research & Development Center, Nippon Zeon Co., Ltd., 1−2−1 Yako, Kawasaki-ku, Kawasaki-shi, Kanagawa 210-8507, Japan.
§ Present address; Department of Polymer Science and Engineering, Kyoto Institute of Technology, Matsugasaki, Sakyo-ku, Kyoto 606-8585, Japan.
∥ Present address; The Institute of Physical and Chemical Research (RIKEN), Structural Biophysics Laboratory, 1-1-1 Kouto, Mikaduki, Sayo, Hyogo 679-5143, Japan.
⊥ Department of Polymer Chemistry, Graduate School of Engineering.

10.1021/ma990437v CCC: $18.00
Published on Web 09/29/1999

into deionized water (4.5 mL). After addition of 0.4% AP aqueous solution (0.5 mL) to initiate the reaction, the pregel solution was quickly transferred into the cell, which was assembled with two round glass plates (22 mm o.d., 0.17 mm in thickness), a ring spacer (0.5 mm in thickness), and a holder. Then, the cell loaded with the pregel solution was immersed into a temperature-controlled water bath for 1 h for gelation at a given temperature. Conversions of NIPAAm were more than 99% for all the gelation systems irrespective of the gelation temperatures employed in the present study. In this way the gels were prepared at various temperatures. The disk-shaped gels thus obtained in the cells were used for the microscope observation. The degree of swelling of the gels was calculated from the ratio of the diameters of the swollen (or deswollen) gels to those of as-prepared gels.

3. Laser Scanning Confocal Microscope Observation. The internal structures of the gels were observed on the as-prepared gel specimen enclosed in the disk-shaped cell at room temperature (about 23 °C) by a laser scanning confocal microscope (LSCM) (Carl-Zeiss LSM410) equipped with Ar (488 nm) and UV (364 nm) lasers. The objective was a water immersion lens with 40 times of magnification and 1.2 as numerical aperture (Carl-Zeiss Apochromat 40× W). Ar and UV lasers were used as incident beams for taking LSCM images under a reflection mode (denoted hereafter as reflection LSCM image) and under a fluorescence mode (denoted hereafter as fluorescence LSCM image), respectively. To observe images of internal structures of the gel under fluorescence mode, the fluorescent probe (ANSA) was introduced into the gel by immersing it in the salt aqueous solution (70 mM) for 3 days. In this case, the internal structures of the gel were observed in the swollen state.

The time to take one sliced LSCM image consisting of 512 × 512 pixels^2 normally required 17 s in the present work. The size of the pixel was 0.1563 × 0.1563 μm^2, and the dynamic range of the intensity was 8 bits. The images were taken by checking the histogram of the intensity so that the maximum and minimum intensities were covered within the range of 8 bits. No image processing was conducted for all the sliced images shown in this work. The image processing was done only for the construction of the three-dimensional internal structures of the gel, as will be discussed in the next section. To construct the three-dimensional internal structures, 80 sliced LSCM images were taken at every 0.5 μm interval along the depth direction. The focal depths were estimated to be about 0.77 μm for the reflection LSCM image and about 1.3 μm for the fluorescence LSCM image in this study.[19]

4. Image Processing for Three-dimensional Image Construction. In this study, we focused on an image construction for the three-dimensional (3D) internal structures of gels on a mesoscopic scale. To construct the 3D image, the following three-step image processing was applied to the observed original reflection LSCM images to make it smooth and make it suitable for a binarization. The original reflection LSCM images are composed of many small bright and gray spots, which may suggest the presence of fine structures. It should be noted, however, that the fine structures are coarse-grained in the course of the image processing for construction of the 3D image in order to highlight the spatial distribution of the network-rich and -poor regions in the gels at mesoscopic scale.

At first, the mean-filter was applied to a series of observed original reflection LSCM images. The intensity of a given pixel at (i, j, k) is defined by $I_0(i, j, k)$ for the original image, $I_1(i, j, k)$ for the image after the first step (mean filtering), $I_2(i, j, k)$ for the image after the second step (median filtering) and $I_3(i, j, k)$ for the image after the third step (smoothing filtering), where i and j denote the pixel position along the x axis and along the y axis in a given slice image, respectively, and k denotes the pixel position along the z axis, that is, the depth direction. $I_1(i, j, k)$ was calculated by

$$I_1(i, j, k) = \frac{\sum_l \sum_m \sum_n W(l, m, n)\, I_0(i + l, j + m, k + n)}{\sum_l \sum_m \sum_n W(l, m, n)} \quad (1)$$

where $W(l, m, n)$ is a weighting function given by

$$W(l, m, n) = \begin{bmatrix} 1, & \text{if } \dfrac{l^2}{4^2} + \dfrac{m^2}{4^2} + \dfrac{n^2}{3^2} < 1 & \text{(2a)} \\ 0, & \text{otherwise} & \text{(2b)} \\ & (l, m, n; \text{integer}) & \end{bmatrix}$$

Note that the number of points (l, m, n) satisfying $(l^2/4^2) + (m^2/4^2) + (n^2/3^2) < 1$ are 97. This mean filtering was applied primarily to smear out or coarse-grain the fine structures composed of the brilliant spots existing in the regions rich in the polymer networks. The filter is, therefore, useful to highlight the regions rich and poor in the polymer networks in the gels.

In the second step, we took the median value ($I_2(i, j, k)$) at the same point (i, j, k) among the mean-filtered intensities $I_1(i + l, j + m, k + n)$ obtained at various points (l, m, n) satisfying $(l^2/4^2) + (m^2/4^2) + (n^2/3^2) < 1$. This median filtering was conducted to effectively eliminate speckled noises which typically appeared as isolated brilliant spots in the dark medium.

At the third step, $I_3(i, j, k)$ is given by

$$I_3(i, j, k) = \frac{\sum_l \sum_m \sum_n W(l, m, n)\, I_2(i + l, j + m, k + n)}{\sum_l \sum_m \sum_n W(l, m, n)} \quad (3)$$

but the weighting function is given by Gaussian function characterized below, instead of eqs 2a and 2b.

$$W(l, m, n) \approx \exp[-(l^2 + m^2 + a^2 n^2)/2\sigma^2] \quad (4)$$

where $a = 1.5$ and $\sigma = 2.2$ pixel. This Gaussian smoothing or filtering was applied mainly to smooth interface roughnesses between the bright and dark domains in the images obtained after the image processing.

Then, each sliced image was binarized using the threshold value obtained by taking account of the intensity histogram of the images with respect to $I_3(i, j, k)$. The binarized cross-section images were computationally stacked, and the interface was traced by the aid of computer to construct the three-dimensional figure.[18]

III. Results

1. Appearance of the Gels. NIPAAm gels were prepared at 20.0, 24.5, 27.0, 32.0, and 38.0 °C. At a certain period of time after the immersion of the cell into water bath, opacity was observed in the systems subjected to gelation at temperatures higher than or equal to 24.5 °C. The opacity of the gels observed during the gelation did not disappear even after cooling the gel below 24.5 °C, as Rathjen et al. reported.[20] Figure 1 shows photograph of the resultant poly(NIPAAm) gels in the cells. The gel prepared at 20.0 °C (part a) was transparent, while the gel prepared at 24.5 °C (part b) was translucent. With increasing preparation temperature, the degree of the opacity increased. The color of the gels prepared at high temperatures such as 32.0 and 38.0 °C was almost milky white as shown in parts d and e of Figure 1. The fact that the opacity of the gels prepared at high temperatures did not disappear at low observation temperatures indicates the presence of

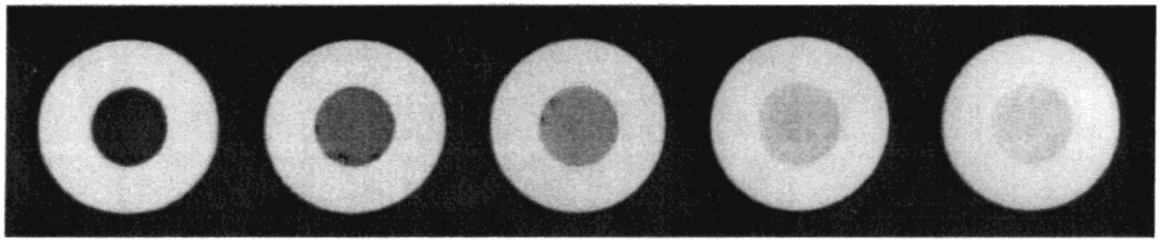

Figure 1. Appearance of poly(NIPAAm) gels. The center parts are gels as prepared and the outer white rings are the cell holders for gelation. Preparation temperatures: (a) 20.0 °C; (b) 24.5 °C; (c) 27.0 °C; (d) 32.0 °C; (e) 38.0 °C, Swelling ratio: 1.0. Other preparation conditions: [NIPAAm] = 1.33 M; [BIS] = 10.0 mM; water. The photograph was taken at room temperature (about 23 °C).

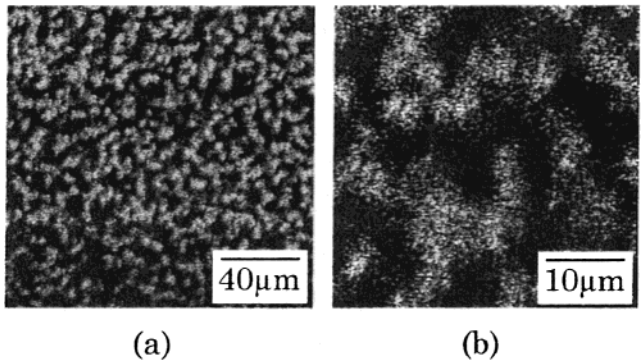

Figure 2. Reflection LSCM images of poly(NIPAAm) gel at different magnifications. The images were taken at a depth of 17.5 μm from the gel surface (swelling ratio: 1.0). Preparation conditions: [NIPAAm] = 1.33 M; [BIS] = 10.0 mM; 27.0 °C; water.

permanent inhomogeneities trapped in the gel by cross-linking (fixed inhomogeneities).

2. LSCM Observation and Identification of the Images. LSCM was applied to observe internal structures of the gels by the irradiation of the Ar laser (488 nm) as an incident beam. The reflection LSCM image of the transparent gel prepared at 20.0 °C had a contrast which is too low to be analyzed. However, the translucent gels exhibited the clear reflection LSCM images. Figure 2 demonstrates a representative reflection LSCM images observed on the gel prepared at 27.0 °C. The images showed a rather regular pattern consisting of **dark** and **bright areas**. Inside the bright areas, there seems to be a number of small **brilliant spots** as clearly seen in the enlarged image (part b), which will be discussed later.

To identify the origin of the dark and the bright areas in the reflection LSCM images, a fluorescent LSCM mode was applied to the gel system to which the ANSA probe had been doped. ANSA is a probe which emits fluorescent light, only when the ANSA molecules locate in hydrophobic circumstance.[21] Therefore, ANSA enables us to identify the hydrophobic domain. Figure 3 shows a comparison of the fluorescence LSCM image (a) and the reflection LSCM image (b) at the same position. For the observation of the fluorescence image, a band path filter (450−490 nm) was employed to detect only emitted fluorescent light. The bright areas in Figure 3a are regions where the fluorescent light emits upon irradiation by the incident UV laser beam. On the basis of the characteristics of the ANSA molecules, the bright areas in the fluorescence LSCM image were found to be the hydrophobic regions. Since the network polymer, namely poly(NIPAAm), has hydrophobic isopropyl groups as side chains, the hydrophobic regions in the gel were identified to be the domains dense in the polymer networks. Likewise, the dark areas in the fluorescence LSCM image were identified to be the domains sparse in the polymer networks.

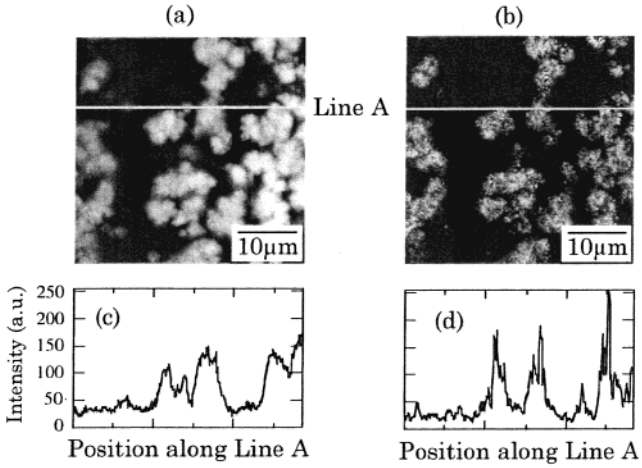

Figure 3. Comparison of a fluorescence LSCM image with a reflection LSCM image of poly(NIPAAm) gel doped with ANSA (swelling ratio: 4.1). Key: (a) fluorescence LSCM image; (b) reflection LSCM image; (c) intensity profile along line A in the LSCM image of part a; (d) intensity profile along line A in the reflection LSCM image of part b. Preparation conditions: [NIPAAm] = 0.126 M; [BIS] = 4.74 mM; 38.0 °C; water.

The reflection LSCM image captured at the same position in the gel as the fluorescence one was also shown in Figure 3b. The pattern of the bright areas in the reflection LSCM image was almost identical to that in the fluorescence LSCM image. More quantitatively, the intensity profiles along the line A in those two LSCM images were similar to each other except for the broadness of the peaks in the fluorescent one due to smearing, as shown in parts c and d. The smearing may be due to Brownian motion of the fluorescent probe molecules, which will make the area of the fluorescent light emission larger than the real area of the network dense region. Thus, the origin of the contrast in the reflection LSCM image is well understood as a **scattering-induced contrast**: The network-rich regions scattered light more strongly than the network-sparse regions, giving rise to the observed bright and dark contrast.

The time dependence of the LSCM image was examined to clarify whether the domains due to the concentration difference in the polymer networks are static or dynamic objects. Figure 4 shows the representative time variations of the reflection LSCM images taken at the same position in the gel.

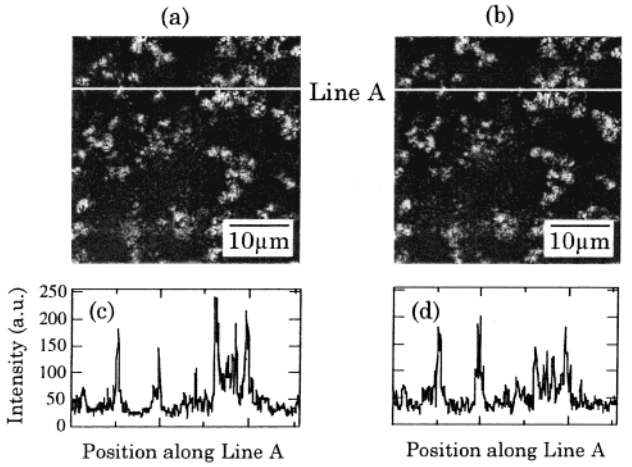

Figure 4. Time dependence of LSCM images (swelling ratio: 4.3). Key: (a) original reflection LSCM image; (b) reflection LSCM image taken at ca. 5 min after the original one was taken; (c) intensity profile along line A in the LSCM image of part a; (d) intensity profile along line A in the LSCM image of part b. Preparation conditions: [NIPAAm] = 0.126 M; [BIS] = 4.74 mM; 38.0 °C; water.

If the domains are dynamic, we can expect that the pattern of the image will easily change with time, when the network polymer concentration of the gel is low. In this work, we deliberately lowered the concentration of NIPAAm monomer for the gelation to reduce the network polymer concentration of the gel. As typically demonstrated in parts a and b of Figure 4, the patterns taken at different times were almost identical to one after another, and the intensity profiles along the line A shown in parts c and d of Figure 4 are well correlated, irrespective of the difference in the observation time over the time scale of our observation (~10 min). These facts indicate that the pattern is static, at least over the time scale of our experiments.

Thus, it is concluded that the reflection LSCM image showed static internal structures in the gel due to fixed concentration fluctuations in the polymer networks.

3. Effect of Preparation Temperatures on the Internal Structures of the Gel. The degree of opacity of the gels increased with the preparation temperatures as shown in Figure 1. To clarify this phenomenon, effects of the preparation temperature on the internal structures were investigated. Figure 5 shows the reflection LSCM images of the gels prepared at 24.5, 27.0, 32.0, and 38.0 °C. The image of the gel prepared at 24.5 °C (part a) is similar to that at 27.0 °C (part b) except for the difference in the width of bright regions. On the other hand, the gels prepared at high temperatures such as 32.0 (part c) and 38.0 °C (part d) showed the images covered by lots of brilliant small spots on the dark background. These facts indicate that the brilliant spots composing the regions dense in polymer networks are easily produced at high temperatures, which will be related to the opacity of the gels.

4. Three-dimensional Domain Structures of the Gel. The gel is a bulk material connected by the cross-linking points and is swollen by a fluid, which is a different state from linear polymer solutions. Three-dimensional (3D) internal structures of the gel were constructed by computationally stacking a series of the sliced reflection LSCM images. Before stacking, each sliced image was binarized after the image processing as described in section II-4. For the comparison, the original image, the image after the image processing and its binarized image were shown in Figure 6 together with their histograms for the intensity distributions of the images. The histogram (e) for the image after the image processing seems to consist of a high narrow peak and a low broad hill. For the binarization of the sliced images, the intensity value of 109 (shown by an arrow) was taken as a threshold.[22] The threshold value did not depend on the images taken at different depth in the gel. The shape of the bright areas in the original LSCM image (a) is conserved in the binarized image (c). However, the small bright spots in the bright and dark areas are coarse-grained in the images b and c, which is useful for highlighting the network-dense and -sparse regions in the gels.

Figure 7 shows the 3D pictures constructed by using a series of the sliced reflection LSCM images observed on the gel prepared at 27 °C. Usually fluorescent images are used for binarization, but in this study, the reflection LSCM images were employed for binarization, since the small amount of heat coming from the fluorescent probe irradiated by the UV laser beam affected the internal structure of the temperature-sensitive gel. Both the dense polymer network domains represented by the bright region in Figure 7a and the sparse polymer network domains represented by the bright region in Figure 7c clearly demonstrate the three-dimensionally connected domain structures, that is, a bicontinuous structure. It should be noted that the patterns shown in parts a and c of Figures 7 are complementary to each other. The interface between these two domains was traced in Figure 7b in which one side of the interface is shown by the brightness and the other side by the darkness. It was found for the first time that the gel

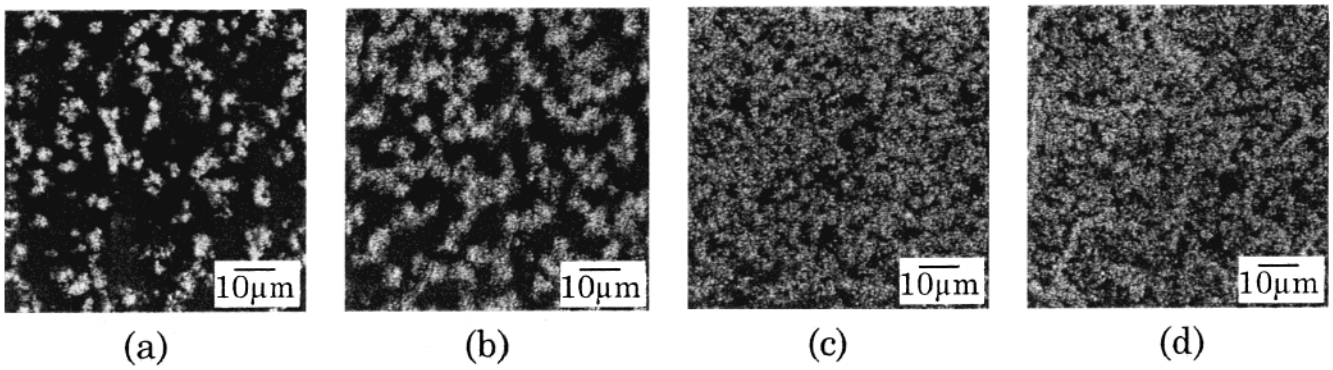

Figure 5. Effect of preparation temperature on the internal structure of poly(NIPAAm) gels (swelling ratio: 1.0). Preparation temperatures: (a) 24.5 °C; (b) 27.0 °C; (c) 32.0 °C; (d) 38.0 °C. Other preparation conditions: [NIPAAm] = 1.33 M; [BIS] = 10.0 mM; water.

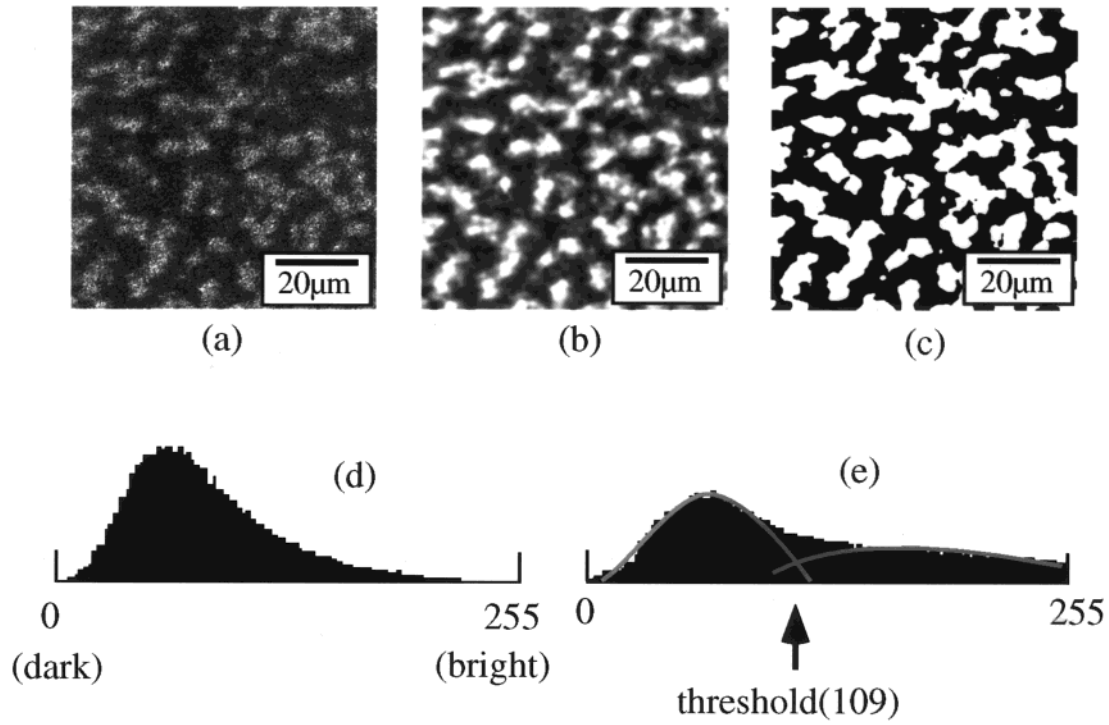

Figure 6. Image processing of reflection LSCM images. Key: (a) original reflection LSCM image; (b) image obtained after the image processing of part a as described in the text; (c) binarized image of part b; (d) histogram for the intensity distribution in original image a; (e) histogram for the intensity distribution in image b.

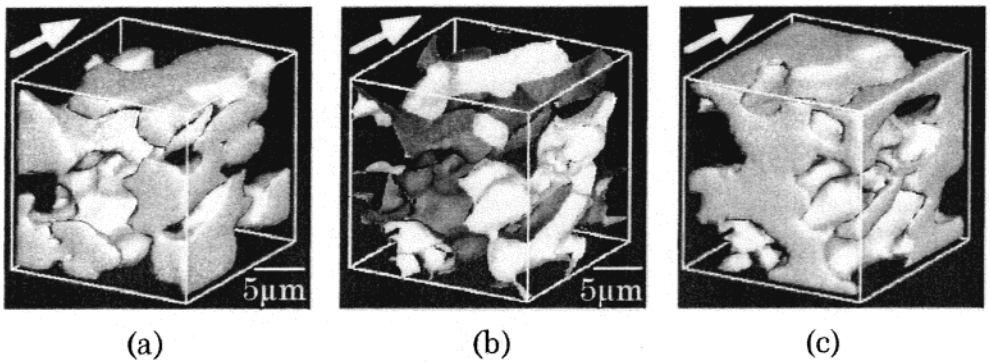

Figure 7. Constructed 3D pictures of poly(NIPAAm) gel. The arrow denotes the direction of depth. Key: (a) bright solid part representing the domain dense in polymer network; (b) interface between dense and sparse polymer network domains, where one side of the interface is shown bright and the other side is shown dark; (c) bright solid part representing the domain sparse in polymer network. Preparation conditions: [NIPAAm] = 1.33 M; [BIS] = 10.0 mM; 27.0 °C, water.

had a bicontinuous domain structure consisting of domains dense and sparse in the polymer network on a mesoscopic scale.

Figure 8 shows the constructed 3D picture indicating the internal structure of the gel prepared at 27.0 °C (part a) and its Fourier Transformation (FT) profile (part b). The structure factor ($S(q)$) of the 3D image (Figure 8a) was obtained by three-dimensional FT. Then $S(q)$ was circular-averaged in the q_x-q_y plane, where q_x and q_y denote the x and y components of the wave vector $\vec{q}$. $S(q)$ thus obtained was double-logarithmically plotted as a function of wavenumber (q) in Figure 8b. Here, q is a wavenumber calculated by $q = 2\pi i/NL$, where i is $0 \sim N/2$, N is the number of the pixels along the x or y axis of the image ($N = 512$ in this case), and L is the lateral length of one pixel. The FT profile exhibited the peak at $q \cong 5 \times 10^{-4}$ nm^{-1}, suggesting the presence of the periodic length between the domains being about 12 μm in the internal structure of the gel. The slope of log $S(q)$ vs q at $q \geq 1$ μm^{-1} in Figure 8 was -4 due to the binarization of the images. Note that the corresponding slope for the gray scale images (before the binarization) showed the slope shallower than -4 (ca. -2.5), due to a spatial (fractallike) distribution of brilliant spots. However the peak position did not depend either on the binarization or on the threshold level for the binarization.[23]

Discussion

Polymer gels consist of three main components, that is, a network polymer, cross-linking points, and fluids. Among these three components, the cross-linking points play an important role on the internal structures of a gel. Figure 9 shows schematic illustrations of the typical network structures in the gels. Parts a and b of Figure 9 show the ideal networks consisting of polymers with the same molecular weight between the cross-linking points. The only difference in parts a and b of Figure 9 is recognized to be a difference in the spatial distribution of the cross-linking points caused by the thermal concentration fluctuations. However, this type of inhomogeneity is dynamic, and the inhomogeneities revers-

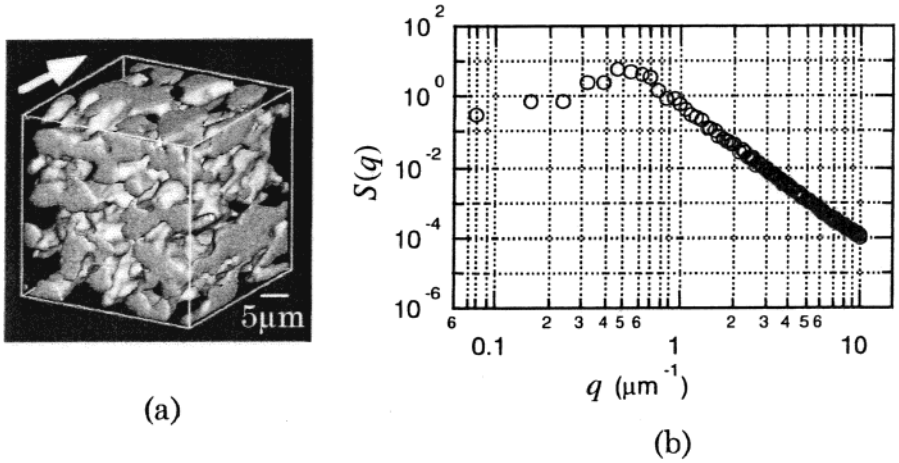

Figure 8. Estimation of the periodical length of the domain dense (or sparse) in polymer networks. Key: (a) 3D picture of internal structure constructed using a series of binarized reflection LSCM images of poly(NIPAAm) gel prepared at 27.0 °C, where the arrow denotes the direction of depth and other preparation conditions are the same as in Figure 7; (b) FT profile calculated from the 3D picture shown in part a.

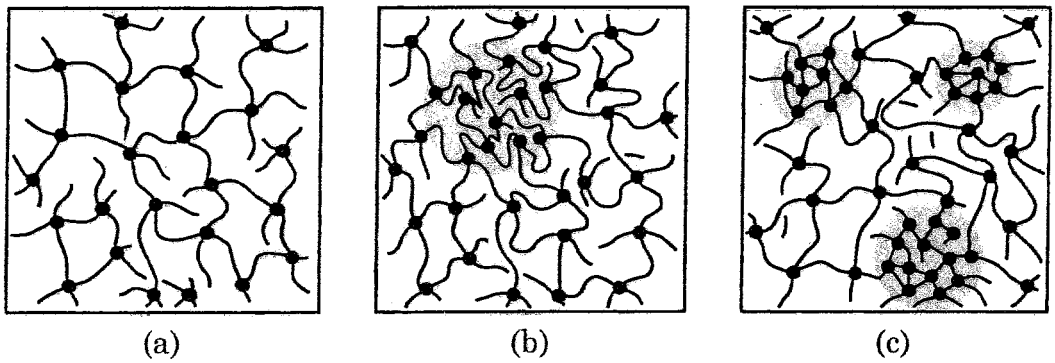

Figure 9. Schematic illustrations of network structures of gels. Curved lines indicate network polymers and black dots cross-linking points. Shaded parts denote the regions rich in network polymers. Key: (a) ideal networks at a homogeneous state; (b) ideal networks at a dynamically inhomogeneous state; (c) real networks having fixed heterogeneities.

ibly appear and disappear: When external conditions such as temperature are varied, the inhomogeneities will change in terms of both amplitude and a spatial extent of the fluctuations as well as the relaxation time. The concentrated region shown by the area shaded in part b, for example, appears (corresponding to a change from part a to b) and disappears (a change from part b to a) with a certain relaxation time.

There is another type of inhomogeneity schematically shown in Figure 9c. The molecular weight between the cross-linking points has a broad distribution, and the local concentration of the cross-linking points spatially fluctuates from place to place in the gel. The shaded blobs in part c schematically illustrate the areas where the average molecular weights between the cross-linking points are low and the concentrations of polymer network trapped by the cross-linking points are high compared with their surrounding regions. The surrounding regions are composed of the networks with higher molecular weights between the neighboring cross-linking points and hence have a lower concentration of the polymer networks. The blobs may correspond to the small brilliant spots observed in the bright domains of the original reflection LSCM images shown in Figures 2−6. These concentration fluctuations are fixed and supposed to be one of the main factors causing the internal structures of the gel. In the 3D bicontinuous domain structures as elucidated in Figures 7 and 8, the domains dense in the networks (bright domains in the reflection LSCM image) are those containing many blobs, while the domains sparse in the network are those containing only a small number of the blobs.

Translucent and opaque poly(NIPAAm) gels prepared at 24.5, 27.0, 32.0, and 38.0 °C showed the static pattern of the reflection LSCM images due to the fixed local concentration fluctuations (the static inhomogenieties) in polymer network. This static pattern is considered to be composed of fundamental units (blobs) as illustrated by Figure 9c. On the other hand, the transparent gel prepared at 20.0 °C did not show any reflection LSCM images with significant contrast, indicating that the gel was rather homogeneous at least at the length scale of visible light. The variation in the static homogeneities caused by the difference in the gelation temperatures will be related to a temperature difference between the preparation temperature and the cloud point (about 32 °C) of an aqueous solution of poly(NIPAAm) that is the main component of the network. When the gel was prepared at a temperature close to or above the cloud point of the poly(NIPAAm) aqueous solution, the thermal concentration fluctuations of the polymer produced in the gelation process are quite large, and sometimes the polymers will start phase-separating before the system is effectively cross-linked. The bicontinuous structure of the poly(NIPPAm) gels found at higher preparation temperatures is considered to be a consequence of the large thermal concentration fluctuations or phase separation followed by the fixation of the fluctuations with the cross-linking. Further studies of the gelation mechanism deserve future work.

The bright regions in the LSCM images observed in the translucent and opaque gels seemed to consist of small brilliant spots. The number of the small brilliant spots increased as the preparation temperature increased. This fact may suggest that the gel has structures much finer than the bicontinuous domain structures shown in Figures 7 and 8, intriguing hierarchy structures of which are now under investigation.[23]

References and Notes

(1) Shibayama, M.; Tanaka, T. *Adv. Polym. Sci.* **1993**, *109*, 1.
(2) Hirotsu, S. *Phase Transitions* **1994**, *47*, 183.
(3) Weiss, N.; Silberberg, A. *Br. Polym. J.* **1977**, *9*, 144.
(4) Hsu, T.-P.; Ma, D. S.; Cohen, C. *Polymer* **1983**, *24*, 1273.
(5) Mallam, S.; Horkay, F.; Hecht, A.-M.; Geissler, E. *Macromolecules* **1989**, *22*, 3356.
(6) Tokuhiro, T.; Amiya, T.; Mamada, A.; Tanaka, T. *Macromolecules* **1991**, *24*, 2936.
(7) Mendes, E., Jr.; Lindner, P.; Buzier, M.; Boue, F.; Bastide, J. *Phys. Rev. Lett.* **1991**, *66*, 1595.
(8) Tokita, M.; Tanaka, T. *J. Chem. Phys.* **1991**, *95*, 4613.
(9) Suzuki, Y.; Nozaki, K.; Yamamoto, T.; Itoh, K.; Nishio, I. *J. Chem. Phys.* **1992**, *97*, 3808.
(10) Rubinstein, M.; Leibler, L.; Bastide, J. *Phys. Rev. Lett.* **1992**, *68*, 405.
(11) Shibayama, M.; Tanaka, T.; Han, C. C. *J. Chem. Phys.* **1992**, *97*, 6829.
(12) Shibayama, M.; Tanaka, T.; Han, C. C. *J. Chem. Phys.* **1992**, *97*, 6842.
(13) Sato, E. S.; Orkisz, M.; Sun, S.-T.; Li, Y.; Tanaka, T. *Macromolecules* **1994**, *27*, 6791.
(14) Shibayama, M.; Morimoto, M.; Nomura, S. *Macromolecules* **1994**, *27*, 5060.
(15) Tokita, M.; Miyoshi, T.; Takegoshi, K.; Hikichi, K. *Phys. Rev.* E **1996**, *53*, 1823.
(16) Suzuki, A.; Yamazaki, M.; Kobiki, Y. *J. Chem. Phys.* **1996**, *104*, 1751.
(17) Wilson, T. *Confocal Microscopy*; Academic Press: London, U.K., 1990.
(18) Nishikawa, Y.; Jinnai, H.; Koga, T.; Hashimoto, T.; Hyde, T. *Langmuir* **1998**, *14*, 1242.
(19) Ishidate, F. *Kenbikyo-no-tsukaikata-note*; Nojima, H., Ed.; Yodoshya: Tokyo, Japan, 1997; p 145. In this note, the following equation was used in order to calculate the vertical (z axis) resolution (fwhm): fwhm [μm] = c\{[2n/(M(N.A.))]-P[dig] + $n\lambda$(EXC)/((N.A.) × (N.A.)) × exp\{−[2(N.A.)/(λ(EXC)-M)]P[dig]\}. Here c is 1.41 × λ(EM)/λ(EXC) for the fluorescent mode and 1 for the reflection mode, λ(EM) is the wavelength of emitted light, λ(EXC) is the wavelength of the incident light, N.A. is the numerical aperture of the objective, M is the magnification of the objective, n is the refractive index of medium, and P[dig] is a special numerical value assigned to the pinhole used.
(20) Rathjen, C. M.; Park, C.-H.; Goodrich, P. R.; Walgenbach, D. D. *Polym. Gels Networks* **1995**, *3*, 101.
(21) Saucier, A. C.; Mariotti, S.; Anderson, S. A.; Purich, D. L. *Biochemistry* **1985**, *24*, 7581.
(22) The histogram (e) in Figure 6 was analyzed to be composed of two Gaussian curves, and the threshold value (109) was easily found as the value of crossing point of the two Gaussian curves.
(23) Okamoto, T.; Hirokawa, Y.; Kimishima, K.; Jinnai, H.; Koizumi, S.; Hashimoto, T. Manuscript in preparation.

MA990437V